MOLECULAR AND CELLULAR BIOLOGY, June 2007, p. 4500–4512 Vol. 27, No. 12
0270-7306/07/$08.00+0 doi:10.1128/MCB.02051-06

Orphan Glutamate Receptor δ1 Subunit Required for High-Frequency Hearing▽

Jiangang Gao,[1]† Stéphane F. Maison,[2]† Xudong Wu,[1] Keiko Hirose,[3] Sherri M. Jones,[4] Ildar Bayazitov,[1] Yong Tian,[1] Guy Mittleman,[5] Douglas B. Matthews,[5] Stanislav S. Zakharenko,[1] M. Charles Liberman,[2] and Jian Zuo[1]*

Department of Developmental Neurobiology, St. Jude Children's Research Hospital, Memphis, Tennessee[1]; Department of Otology and Laryngology, Harvard Medical School and Eaton-Peabody Laboratory, Massachusetts Eye & Ear Infirmary, Boston, Massachusetts[2]; Department of Otolaryngology, Cleveland Clinics Foundation, Cleveland, Ohio[3]; Department of Communication Sciences and Disorders, East Carolina University, Greenville, North Carolina[4]; and Department of Psychology, University of Memphis, Memphis, Tennessee[5]

Received 2 November 2006/Returned for modification 29 November 2006/Accepted 6 April 2007

The function of the orphan glutamate receptor delta subunits (GluRδ1 and GluRδ2) remains unclear. GluRδ2 is expressed exclusively in the Purkinje cells of the cerebellum, and GluRδ1 is prominently expressed in inner ear hair cells and neurons of the hippocampus. We found that mice lacking the GluRδ1 protein displayed significant cochlear threshold shifts for frequencies of >16 kHz. These deficits correlated with a substantial loss of type IV spiral ligament fibrocytes and a significant reduction of endolymphatic potential in high-frequency cochlear regions. Vulnerability to acoustic injury was significantly enhanced; however, the efferent innervation of hair cells and the classic efferent inhibition of outer hair cells were unaffected. Hippocampal and vestibular morphology and function were normal. Our findings show that the orphan GluRδ1 plays an essential role in high-frequency hearing and ionic homeostasis in the basal cochlea, and the locus encoding GluRδ1 represents a candidate gene for congenital or acquired high-frequency hearing loss in humans.

Ionotropic glutamate receptors include three major families, *N*-methyl-D-aspartate (NMDA), kainate, and α-amino-3-hydroxy-5-methyl-4-isoxazole-4-propionic acid (AMPA) receptors, and a fourth orphan family of delta receptors (GluRδ1 and GluRδ2). GluRδ1 and GluRδ2 share 56% amino acid identity with each other but only 17 to 28% identity with other ionotropic glutamate receptors (25, 45). Neither GluRδ1 nor GluRδ2 can be activated by AMPA, kainate, NMDA, glutamate, or any other ligands when expressed alone or in combination with other subunits in heterologous expression systems (46). Sequence analysis suggests that both GluRδ1 and GluRδ2 are more homologous to non-NMDA receptors; an analysis of GluRδ2 with the Lurcher mutation in the third transmembrane domain suggests that GluRδ2 functions as an AMPA-like receptor (21, 44, 48). It is expressed exclusively in Purkinje cells of the cerebellum. Targeted disruption of GluRδ2 causes motor coordination impairment, Purkinje cell maturation, and long-term depression of synaptic transmission (20). Subsequently, it was found that the appropriate transport of GluRδ2 to the Purkinje cell surface is required for the function of the receptor in synaptic transmission (15, 46). Recently, it has been suggested that GluRδ2 is the receptor for cerebellin 1, a glycoprotein of the C1q and tumor necrosis factor family that is secreted from cerebellar granule cells (16).

In contrast to GluRδ2, GluRδ1 is expressed in many areas in the developing central nervous system, including the hippocampus and the caudate putamen, but is absent in the cerebellum in guinea pigs, rats, and mice (24–26). In the adult, GluRδ1 is expressed at high levels in hippocampal neurons (24–26), cochlear inner hair cells (IHCs), and spiral ganglia and their satellite cells as well as vestibular hair cells and vestibular ganglia in guinea pigs and rats (36). GluRδ1 is also weakly expressed in Claudius cells in the basal cochlear turns and in vestibular supporting cells (36). In IHCs, GluRδ1 immunostaining appears over the entire cell surface rather than localized to the synaptic sites at the base of the cell (36). Despite these expression patterns, no functional role of GluRδ1 in vivo has been reported.

To investigate its role, we created and characterized a null allele of GluRδ1 in mice. The GluRδ1$^{-/-}$ mice displayed a significant auditory phenotype, demonstrating that GluRδ1 is required for high-frequency hearing and suggesting that it has a role in cochlear ion homeostasis. Function in other cells expressing GluRδ1, such as vestibular hair cells, vestibular ganglia, and hippocampal neurons, was not significantly affected in GluRδ1$^{-/-}$ mice. The locus encoding GluRδ1 thus represents a candidate gene for congenital or acquired high-frequency hearing loss in humans.

MATERIALS AND METHODS

Table 1 summarizes the procedures used in these studies as well as the age and number of mice used for each procedure. Details for each procedure follow.

Construction of the GluRδ1 targeting vector and generation of GluRδ1 mutant mice. We screened a bacterial artificial chromosome library (Research Genetics) containing mouse 129/Sv genomic DNA and obtained overlapping

* Corresponding author. Mailing address: Department of Developmental Neurobiology, St. Jude Children's Research Hospital, Memphis, TN 38105. Phone: (901) 495-3891. Fax: (901) 495-2270. E-mail: jian.zuo@stjude.org.
† These authors contributed equally to this work.
▽ Published ahead of print on 16 April 2007.

TABLE 1. The age, genotype, and number of mice used for each procedure

Procedure	Age (wk)	No. of mice		
		GluRδ1$^{+/+}$	GluRδ1$^{+/-}$	GluRδ1$^{-/-}$
Western blot	8	4	4	4
Immunostaining	8	13	0	12
Histopathology	8	2	0	2
Laser capture microdissection	8	3	0	1
ABR	6–8	4	6	4
DPOAE	6–8	4	6	4
EP	8	7	7	7
ABR post-noise exposure	6–8	6	0	6
DPOAE post-noise exposure	6–8	6	0	6
DPOAE suppression	6–8	3	6	3
Rotarod	8	9	9	9
Swim test	8	9	9	9
VsEP	11–12	10	12	10
Hippocampal morphology	8 and 16	2	0	2
Hippocampal electrophysiology	10–11	4	0	4
Water maze test	8	6	10	11

clones with average sizes of 150 kb. A 7-kb GluRδ1 genomic DNA fragment containing exon 11 (transmembrane domains 1 and 2 [TM1 and TM2]) and another 10-kb fragment containing exon 12 (TM3) were isolated, restriction mapped, and sequenced. TL-1 embryonic stem (ES) cells derived from the 129/SvEv strain were electroporated with linearized targeting vector. DNA from the ES cell line was digested with SpeI and analyzed by Southern blotting (Fig. 1). One homologously recombined targeted cell line was obtained, and subsequent germ line transmission was achieved. We developed a PCR genotyping assay (30 cycles) with a pair of primers from the deleted region of the GluRδ1 gene (5′ GCAAGCGCTACATGGACTAC 3′ and 5′ GGCACTGTGCAGGG TGGCAG 3′) and a pair of primers from the targeting vector (5′ CCTGAAT GAACTGCAGGACG 3′ and 5′ CGCTATGTCCTGATAGCGATC 3′). All mice analyzed were from a mixed background of 129/SvEv and C57BL/6 in the F_2 to F_6 generations. All mouse use protocols were approved by institutional animal care and use committees.

Western blot analyses. To confirm the ablation of the GluRδ1 protein in GluRδ1$^{-/-}$mice, we performed Western blot analysis. Extracts from mouse inner ears, hippocampi, and cerebella containing 50 to 150 μg of protein were separated in a 3 to 8% NuPAGE Tris-acetate polyacrylamide gel (Novex) containing sodium dodecyl sulfate. After transfer, the polyvinylidene fluoride membrane (Immobilon) was treated with primary antibodies (rabbit GluRδ1/2 polyclonal antibody from Chemicon [catalog no. AB1514] and β-actin antibody from Sigma [catalog no. A5441]), horseradish peroxidase-conjugated secondary antibody (Amersham Pharmacia Biotech), and SuperSignal (Pierce).

Immunostaining and histologic analysis. For the evaluation of molecular and morphological changes in GluRδ1$^{-/-}$ mice, mice were anesthetized with Avertin (500 mg/kg of body weight) or ketamine and xylazine (0.72/0.46 mg/30 g of body weight), followed by intracardial perfusions of 0.1 M phosphate-buffered saline and subsequently 4% paraformaldehyde solution in 0.1 M phosphate buffer (pH 7.3). Cochleas were postfixed overnight and then decalcified in EDTA for 1 to 3 days. For whole-mount immunolabeling, cochleas were dissected, permeabilized with 1.0% Triton X-100 for 10 min, and incubated overnight in primary antibodies. The next day, the samples were placed in biotin-labeled secondary antibodies, a complex consisting of avidin, biotin, and horseradish peroxidase (ABC kit; Vector Laboratory), and then incubated in peroxidase substrate. For immunostaining of sections, decalcified cochleas were embedded in paraffin and sectioned into 12-μm thicknesses. Slides were deparaffinized. Nonspecific binding of secondary antibody was blocked by incubation with 10% goat serum in phosphate-buffered saline for 30 min at room temperature. Samples were then incubated in primary and secondary antibodies as described above. Samples were observed under a microscope (Olympus BX60). The primary antibodies used were Chemicon AB1514 for GluRδ1/2, Abnova H00002894-A01, specific for GluRδ1 (for hippocampal immunostaining), Santa Cruz SC22926 for Kir3.1, Sigma P6610 for Kv4.1, Santa Cruz SC16053 for the Na^+-K^+ ATPase β1 subunit (Atp1b1), Santa Cruz SC21547 for the Na^+-K^+-$2Cl^-$ cotransporter (Nkcc1), Chemicon MAB329 for synaptophysin, Sigma V5387 for the vesicular acetylcholine transporter (VAT), Chemicon AB197 for the calcitonin gene-related peptide (CGRP), and Chemicon AB5811P for SNAP25. For the anti-GluRδ1/2 antibody from Chemicon, lots produced before 2002 worked well in our immunostaining and Western blot analyses, but recently produced lots failed in immunostaining. In our hands, the various GluRδ1-specific antibodies (Abnova H00002894-A01 and Abnova H00002894-M01; kindly provided by R. Wenthold) did not result in immunostaining signals that were consistent and different between GluRδ1$^{+/+}$ and GluRδ1$^{-/-}$ cochlear sections despite numerous attempts with a variety of conditions, including antigen retrieval.

For the immunostaining of SNAP25, synaptophysin, CGRP, or VAT, each dissected cochlear piece was measured by computerized planimetry and the cochlear location was converted to the frequency that is normally processed at that location (8). To quantify immunopositive terminals, outlines were traced via a drawing tube using high-numerical-aperture objective lenses (total magnification, ×2,000). During tracing, fine focus was continually adjusted to optimize

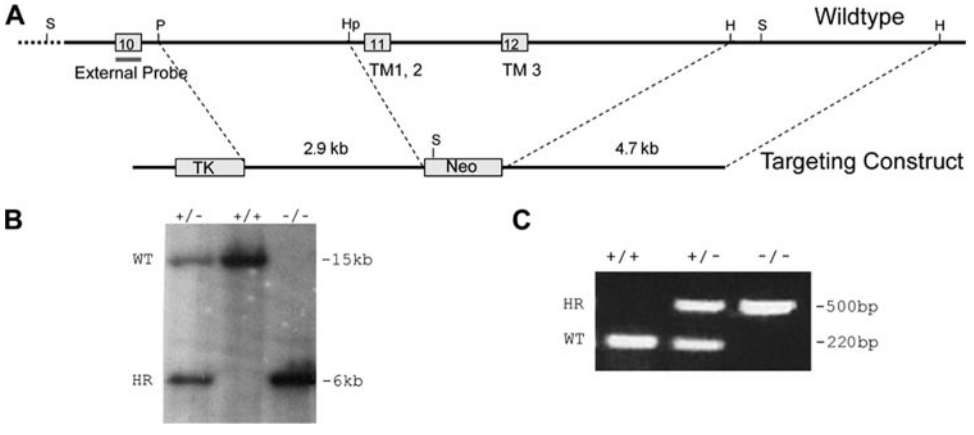

FIG. 1. Targeted disruption of the GluRδ1 locus. (A) Strategy for targeted deletion of the GluRδ1 gene. At the wild-type GluRδ1 locus, the boxes indicate exons 10 to 12; exon 11 encodes the predicted TM1 and TM2, and exon 12 encodes TM3 of GluRδ1 protein. An 8-kb genomic DNA containing exons 11 and 12 is replaced with the PGK-Neo-pA (Neo) cassette in the targeting construct. A 2.9-kb fragment (short arm) and a 4.7-kb fragment (long arm) were used. A new SpeI (S) site in the Neo cassette resulted in a shorter band after homologous recombination on the Southern blot when the external probe from exon 10 was used. H, HindIII; Hp, HpaI; P, PstI. (B) Southern blot analysis of genomic DNA isolated from GluRδ1$^{+/+}$ (+/+), GluRδ1$^{+/-}$ (+/−), and GluRδ1$^{-/-}$ (−/−) mice. SpeI-digested tail DNA was hybridized with the external probe (exon 10). The probe detected 15-kb wild-type (WT) and 6-kb homologous recombined (HR) bands. (C) PCR genotyping assay using a pair of primers (from the deleted region of TM1 to TM3) that amplify a 220-bp band and another pair of primers (from the targeting vector) that amplify a 500-bp band (see Materials and Methods). Note that there is no 220-bp band in the homozygous mouse.

imaging of each terminal cluster. Traces were digitized, and areas were computed using NIH Image software. For the outer hair cell (OHC) area, all immunopositive terminals were traced and values from each row were averaged within bins corresponding to 100 μm of cochlear length.

For an assessment of histopathology, animals were anesthetized, followed by intracardial perfusion with 2.5% glutaraldehyde and 1.5% paraformaldehyde in phosphate buffer. Temporal bones were extracted, and round and oval windows opened for intralabyrinthine perfusion of fixative. Cochleas were then osmicated (1% OsO_4 in dH_2O), decalcified (0.1 M EDTA with 0.4% glutaraldehyde), dehydrated in ethanols and propylene oxide, embedded in Araldite resins, and sectioned at 40 μm on a Historange with a carbide steel knife. Sections were mounted on slides and coverslipped.

Laser capture microdissection of cochlear sections and reverse transcriptase PCR (RT-PCR) analysis. For detailed expression analysis of GluRδ1 in the inner ear, laser capture microdissection was performed using the PixCell II system (Arcturus). We used a previously described method (32) with some modifications. Briefly, the mice were anesthetized and intracardially perfused with 4% paraformaldehyde in phosphate buffer. Temporal bones were removed, and oval windows were opened for the injection of fixative. Cochleas were then postfixed overnight and decalcified in 0.1 M EDTA for 1 to 3 days. The cochleas were dehydrated in ascending concentrations of alcohol and embedded in paraffin. The embedded cochleas were sectioned into 12-μm thicknesses, and sections were mounted on uncharged slides (six sections on each slide). The sections were deparaffinized in xylene and dried at room temperature. We captured inner hair cells, outer hair cells, spiral ganglion cells, type I and IV fibrocytes, Deiters' cells, Claudius cells, Boettcher cells, inner sulcus cells, marginal cells, and vestibular hair cells from eight slides from each mouse. We pooled all of the cells in each category from different slides into a single tube. As a control, we scraped the whole sections from one slide into a tube. Three GluRδ1$^{+/+}$ mice and one GluRδ1$^{-/-}$ mouse were independently analyzed.

We used the Paradise whole-transcript RT reagent system (Arcturus, Mountain View, CA) to purify mRNA from both whole sections and laser-captured cells from cochlear sections. We made cDNA by reverse transcription from the mRNA using the same kit as above. For PCR, we designed four pairs of primers to amplify the cDNA of GluRδ1 (forward, 5′ ACCTCCTGGAATGGGATGAT; reverse, 5′ CCTCAGGCTTCTTGATGAGG), prestin (forward, 5′ AGTGGCT GCCAGCATATAAA; reverse, 5′ CGATGAGTACAGGCCAAACA), p27 (forward, 5′ ATTGGGTCTCAGGCAAACTCT; reverse 5′ GTTCTGTTGGC CCTTTTGTTT), and β-actin (forward, 5′ AATTTCTGAATGGCCCAGGT; reverse, 5′ TGTGCACTTTTATTGGTCTCAA). We used cDNA of P9 whole cochlea as a positive control and mRNA of P9 whole cochlea without reverse transcription as a negative control for PCR.

Assays of cochlear function. For auditory brain stem responses (ABR), distortion product otoacoustic emissions (DPOAE), and endolymphatic potential (EP) measurements, mice were anesthetized with xylazine (20 mg/kg intraperitoneally) and ketamine (100 mg/kg intraperitoneally). For ABR, needle electrodes were inserted at the vertex and pinna, with a ground near the tail. ABR potentials were evoked with 5-ms tone pips (0.5-ms rise-fall with a $\cos^2$ onset envelope, delivered at a rate of 35/s). The response was amplified (10,000 times), filtered (100 Hz to 3 kHz), and averaged with an analog-to-digital board in a LabVIEW-driven data acquisition system. The sound level was raised in 5-dB steps from 10 dB below threshold to a 90-dB sound pressure level (SPL). At each sound level, 1,024 responses were averaged (with stimulus polarity alternated) using an artifact reject system, whereby response waveforms were discarded if the peak-to-peak amplitude exceeded 15 μV. The threshold was defined by visual inspection of stacked waveforms as the lowest SPL at which coherent responses were detectable at a latency consistent across levels.

The DPOAE at distortion frequency $2f_1$-f_2 was recorded with a custom acoustic assembly consisting of two one-quarter-inch condenser microphones to generate primary tones of different frequencies (f_1 and f_2, with $f_2/f_1 = 1.2$ and f_2 level 10 dB $< f_1$ level) and a Knowles miniature microphone (EK3103) to record ear canal sound pressure. Stimuli were generated digitally (National Instruments; catalog no. 6052E), and the maximum level of stimuli for DPOAE was 80 dB SPL. Ear canal sound pressure was amplified and digitally sampled at 4 μs. Fast Fourier transforms were computed from averaged waveforms of ear canal sound pressure, and $2f_1$-f_2 DPOAE amplitude and the surrounding noise floor were extracted. Noise floors ranged from −25 to −5 dB SPL, depending on frequency. Isoresponse contours were interpolated from amplitude-versus-level functions performed in 5-dB steps of primary level.

For EP measurement (on a separate cohort of animals), the bulla was opened, exposing the cochlea, and the bone of the otic capsule over the basal turn was opened using a small knife. The spiral ligament and stria vascularis were left intact. A glass micropipette electrode (20 MΩ) filled with 150 mM KCl was introduced into the opening of the cochlea using a Kopf micropositioner. The signal was amplified 10-fold and read by custom software. The EP was considered valid if (i) there was a rapid rise in voltage (>25 mV per 3-μm advance), (ii) the peak voltage remained stable for 30 s or more, and (iii) the voltage returned to 0 when the electrode was retracted.

Acoustic injury. For the evaluation of the vulnerability of GluRδ1$^{-/-}$ mice to acoustic injury, mice were exposed, awake, and unrestrained, within cages suspended inside a small reverberant sound exposure box. The exposure stimulus was generated by a custom white-noise source, filtered (Brickwall filter with a 60-dB-octave slope), amplified (Crown power amp), and delivered (JBL compression driver) through an exponential horn fitted securely to a hole in the top of a reverberant box. Sound exposure levels were measured at four positions within each cage using a one-quarter-inch Bruel and Kjaer condenser microphone; sound pressure was found to vary by less than 0.5 dB across these measurement positions. Sound pressure was calibrated by positioning the microphone at the approximate position in relation to the animal's head. Mice were exposed for 2 h to the octave band noise (8 to 16 kHz) at 89 dB SPL.

Assays of vestibular function. For vestibular function in GluRδ1$^{-/-}$ mice, we employed various behavioral and electrophysiological vestibular tests. In the Rotarod test, the rod (San Diego Instruments) rotated at speeds increasing in 5-rpm increments from 0 to 20 rpm and the retention time of the mice was recorded. Mice were tested in four trials each day at the same hours of the day over 4 days. For the swim test, each mouse was placed in a glass aquarium filled with tepid water. The time required for the mouse to surface and to maintain a horizontal bodyline swimming at the surface was recorded.

For linear vestibular evoked potential (VsEP) measurements, experimenters were blinded to the genotype during data collection and analysis. Animals were anesthetized (Equithesin, 4 μl/g intraperitoneally), and each skull was prepared with a head mount. A thumbscrew was secured at the midline, and two additional electrodes were placed behind the left and right pinnae with a ground at the ventral neck. The animals were placed supine, and each head was secured to an electromechanical shaker with the naso-occipital axis oriented vertically. Stimuli were linear acceleration pulses (2-ms duration; 16 pulses/s) presented in two directions, normal and inverted. Normal polarity was defined as upward displacement, while inverted stimuli displaced the platform downward. Stimulus amplitude was measured in jerk (i.e., *g*/ms, where 1.0*g* = 9.8 m/s^2 and 1.0*g*/ms = 9.8 μm/ms^3 [18]) using a calibrated accelerometer attached to the shaker platform. To monitor the jerk component of the stimulus, the output of the accelerometer was differentiated electronically. Stimulus amplitude was recorded in dB re: 1.0*g*/ms and ranged from −18 to +6 dB re: 1.0*g*/ms, adjusted in 3-dB steps. Electrophysiologic activity was amplified (200,000-fold) and filtered (300 to 3,000 Hz), and VsEPs to normal and inverted stimulus polarities (1,024 points, 10 μs/point, 128 responses per averaged waveform) were recorded. Four waveforms were obtained at each stimulus intensity level, two for normal polarity stimuli and two for the inverted polarity. Averaging of responses to normal and inverted polarities was completed offline to produce the final averaged waveforms used for analysis. Three response parameters were quantified: threshold, peak latencies, and peak-to-peak amplitudes. The threshold measured in dB re: 1.0 *g*/ms was defined as the stimulus amplitude midway between that which produced a discernible VsEP and that which failed to produce a response. Thresholds, latencies, and amplitudes were compared among the three groups of animals using one-way analysis of variance (ANOVA) (thresholds) and multivariate ANOVA (latencies and amplitudes) with a significance level of P less than 0.05.

Hippocampal electrophysiology. For the evaluation of the role of GluRδ1 in synaptic transmission and synaptic plasticity, hippocampal slices were prepared from GluRδ1$^{-/-}$ and GluRδ1$^{+/+}$ male mice without prior knowledge of mouse genotype. Slices were continuously superfused with artificial cerebrospinal fluid containing 125 mM NaCl, 2.5 mM KCl, 2 mM $CaCl_2$, 2 mM $MgSO_4$, 1.25 mM NaH_2PO_4, 26 mM $NaHCO_3$, and 10 mM glucose, with 95% O_2 and 5% CO_2 at 30 to 31°C (2 ml/min). Schaffer collateral synapses were stimulated with a bipolar tungsten electrode in CA1 stratum radiatum placed 100 to 150 μm from the recording pipette, and field excitatory postsynaptic potentials (fEPSPs) were collected using a MultiClamp 700B amplifier (Molecular Devices). To ensure equivalent activation of postsynaptic neurons in all experiments, stimulation intensities were chosen to evoke an fEPSP with a slope of approximately 1 mV/ms. In long-term potentiation (LTP) experiments, Schaffer collaterals were stimulated at 0.033 Hz before and after the induction of LTP. LTP was induced by a 200-Hz pulse protocol consisting of 10 trains of 200 ms of stimulation at 200 Hz delivered every 5 s at the baseline stimulation intensity. Data were analyzed using Clampfit 9.0 software (Molecular Devices). Results were grouped according to mouse genotype.

Morris water maze test. For an examination of defects in LTP in GluRδ1$^{-/-}$ mice in vivo, mice of three genotypes were tested in a water maze that consisted of a circular blue plastic tank, 160 cm in diameter and 38 cm deep. The maze was located in a large test room surrounded by external cues that could be used for spatial navigation. The tank was filled to 30 cm with water at 21°C made opaque by the addition of a small quantity of nontoxic white paint (tempera). The platform, a 10-cm square of Plexiglas covered with a rough green plastic scouring pad, was mounted on a solid column 1 cm below the surface such that it could not be seen from water level. Four equally spaced points around the edge of the tank were used as start positions and divided the maze into four quadrants. During the acquisition of the place task, the platform was in the middle of one quadrant, equidistant between the center and the outer wall of the maze. Mice were trained for one block of four trials on each of 10 consecutive days. Within each block of trials, all four start positions were used once each in a pseudorandom sequence. For each trial, a mouse was placed in the water facing the wall at the start position. The time required to find the escape platform was recorded. Any mouse failing to find the platform within 60 s was placed on the platform. Approximately 10 min separated the individual trials in each day's block of tests.

RESULTS

Generation of GluRδ1$^{-/-}$ mice. To create GluRδ1$^{-/-}$ mice, we designed a targeting construct that deleted exons 11 and 12 of the GluRδ1 gene (Fig. 1A). This targeted disruption ensured the removal of three of the four transmembrane domains and introduced a frameshift after exon 12. We screened 380 ES cell colonies by genomic Southern blot analysis using an external probe, and one underwent homologous recombination. Using Neo as a probe, we confirmed that there were no other random integrations in this ES cell line (data not shown). We performed karyotyping to determine cytogenetic normality. After blastocyst injection, high chimeras were obtained, and germ line transmission was achieved. The crosses between GluRδ1$^{+/-}$ mice yielded offspring with an approximately 1:2:1 ratio of the GluRδ1$^{+/+}$ (63 offspring), GluRδ1$^{+/-}$ (126 offspring), and GluRδ1$^{-/-}$ (65 offspring) genotypes, suggesting no embryonic lethality in the GluRδ1$^{-/-}$ mice. The correct targeting of GluRδ1 gene was further confirmed by genomic Southern blot analysis of mice with germ line transmission (Fig. 1B). In the PCR analysis, no 220-bp wild-type bands (in the deleted region) were detected in the homozygous mice (Fig. 1C).

To confirm the ablation of the GluRδ1 protein in GluRδ1$^{-/-}$ mice, we performed Western blot analysis with a polyclonal antibody against the C termini of both the GluRδ1 and GluRδ2 proteins. As a positive control for this antibody, we used the cerebellum, where GluRδ2 is predominantly expressed and is unchanged in either GluRδ1$^{+/+}$ or GluRδ1$^{-/-}$ mice (Fig. 2A); because GluRδ2 is not normally expressed in the inner ear or hippocampus (36), this antibody can be used to assay GluRδ1 expression in these tissues from mutant mice. Both GluRδ1$^{+/+}$ and GluRδ1$^{+/-}$ mice expressed the expected ~115-kDa GluRδ1 protein, and no GluRδ1 protein with a mass of 115-kDa or any other size was detected in the inner ear or hippocampus of GluRδ1$^{-/-}$ mice (Fig. 2A). It remains possible that a small N-terminal peptide is made in GluRδ1$^{-/-}$; however, it is likely that this peptide would be degraded due to the lack of proper transmembrane domains and a C terminus, so GluRδ1$^{-/-}$ is therefore an effective null allele.

In addition, we performed immunofluorescence on hippocampus and cerebellum from GluRδ1$^{+/+}$ and GluRδ1$^{-/-}$ mice using a GluRδ1-specific antibody (Fig. 2B; data not shown). GluRδ1 is absent in cerebellum but present in hippocampus of GluRδ1$^{+/+}$ mice; however, it is absent in both regions of GluRδ1$^{-/-}$ mice (Fig. 2B; data not shown), consistent with Western blot results (Fig. 2A). Furthermore, our wild-type immunostaining results are consistent with in situ hybridization results reported recently for developing and adult mouse brains (24, 26). Our Western blotting and immunostaining results also demonstrated that GluRδ2 is absent in the inner ear and hippocampus and that no obvious up-regulation of GluRδ2 occurs in the cerebellum, hippocampus, or inner ear of GluRδ1$^{-/-}$ mice.

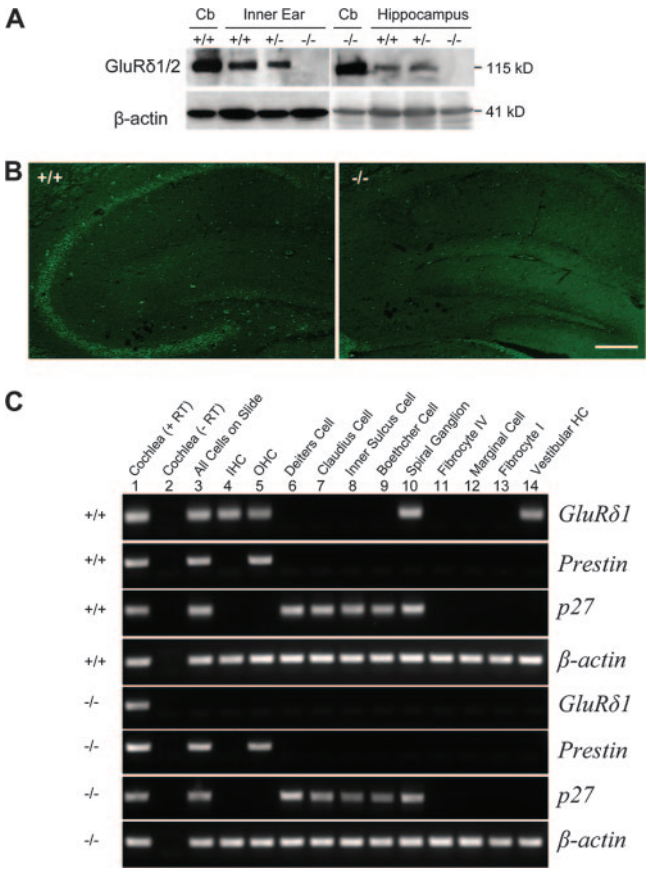

FIG. 2. Ablation of GluRδ1 in GluRδ1$^{-/-}$ mice. (A) Western blot analysis of inner ear, hippocampal, and cerebellar homogenates from GluRδ1$^{+/+}$ (+/+), GluRδ1$^{+/-}$ (+/−), and GluRδ1$^{-/-}$ (−/−) mice. The GluRδ1/2 antibody detected an ~115-kDa band seen in cerebella (Cb) of GluRδ1$^{+/+}$ and GluRδ1$^{-/-}$ mice (representing GluRδ2) and hippocampi and inner ears of GluRδ1$^{+/+}$ and GluRδ1$^{+/-}$ mice (representing GluRδ1) but did not detect any band in GluRδ1$^{-/-}$ mice. Anti-β-actin antibody was used as control. (B) Immunofluorescence of hippocampal sections of a GluRδ1$^{+/+}$ mouse and a GluRδ1$^{-/-}$ mouse at 2 months of age. The GluRδ1-specific antibody detected signals in hippocampal neurons in the GluRδ1$^{+/+}$ mouse, but not in the GluRδ1$^{-/-}$ mouse. The bar (50 μm) applies to both panels. (C) RT-PCR analysis of different laser-captured cells from the mouse cochlear sections of GluRδ1$^{+/+}$ and GluRδ1$^{-/-}$ mice. Lane 1, positive control cDNA of P9 whole cochlea with reverse transcription. Lane 2, negative control cDNA of P9 whole cochlea without reverse transcription. Lane 3, cDNA of all cells from the entire cochlear section. Lanes 4 to 14, cDNAs of laser-captured individual cell types. Genotypes of mice are labeled on the left. Genes for specific cell types used for RT-PCR are labeled on the right. Primers for GluRδ1 were from the deleted exons.

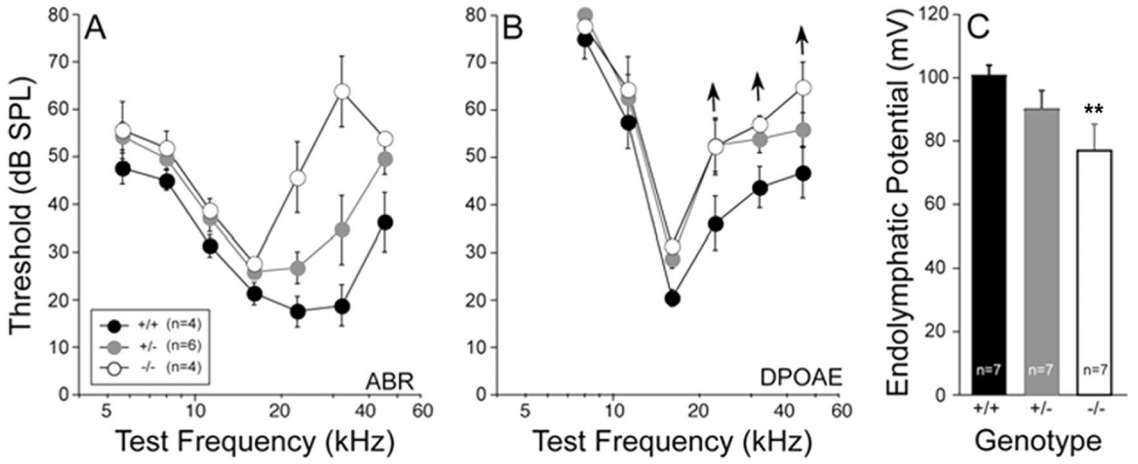

FIG. 3. Cochlear thresholds are elevated at high frequencies in GluRδ1$^{-/-}$ (−/−) mice (A and B), and the EP is reduced in the basal turn (C). GluRδ1$^{+/-}$ (+/−) animals show intermediate values by all measures. Panels A and B show ABR and DPOAE data, respectively, for the same cohort of animals; panel C is from a separate group. Means and standard errors (error bars) are shown; numbers of animals ("*n*") in each group are given. Statistical analyses are described in the text. Arrows on DPOAE points from GluRδ1$^{-/-}$ mice indicate that these values are minimum estimates because some ears showed no response at the highest sound levels (80 dB SPL). The double asterisks in panel C represent a significant difference (P was <0.01 by Student's t test; P was <0.05 by one-way ANOVA) between GluRδ1$^{+/+}$ and GluRδ1$^{-/-}$ mice, while other group comparisons showed insignificant differences.

GluRδ1$^{-/-}$ mice showed no obvious developmental or behavioral abnormality, except for overall weight reductions by 4 months of age. In all of the groups at 2 months of age or younger, weight differences were not significant (data not shown). At 4 months, the weights of male GluRδ1$^{-/-}$ mice were approximately 89% of those of the GluRδ1$^{+/+}$ males, and the weights of female GluRδ1$^{-/-}$ mice were approximately 87% of those of the GluRδ1$^{+/+}$ females; there was no significant difference between the weights of GluRδ1$^{+/-}$ and GluRδ1$^{+/+}$ mice of either sex.

Cochlear GluRδ1 expression. To independently verify the expression of GluRδ1 in specific single cell types of the inner ear of GluRδ1$^{+/+}$ mice and to confirm the deletion of GluRδ1 in the inner ear of GluRδ1$^{-/-}$ mice, we used laser capture microdissection and RT-PCR (Fig. 2C). Prestin (an OHC-specific marker), p27 (a supporting cell marker), and β-actin (a ubiquitous marker) were used as controls. GluRδ1 was expressed in IHCs, OHCs, spiral ganglia, and vestibular HCs. However, it was not expressed in type I and IV fibrocytes, Deiters' cells, Claudius cells, inner sulcus cells, Boettcher cells, or marginal cells in stria vascularis (Fig. 2C). Our results are largely consistent with those of a previous report (36); however, some differences exist: in previous studies, OHCs were negative in both in situ and immunostaining analyses for both guinea pigs and rats, whereas Claudius cells in basal turns were negative in rat cochleae by in situ analysis but weakly positive in guinea pig cochleae by immunostaining analysis with only anti-GluRδ1 antibody (see Fig. 2 and 5 in reference 36). Such differences are subtle and can be subject to differences between species or in sensitivities of detection methods. In the inner ears of GluRδ1$^{-/-}$ mice, the corresponding portion of GluRδ1 mRNA was indeed deleted in all cell types analyzed (Fig. 2C). These results were reproduced in three independent experiments using different GluRδ1$^{+/+}$ and GluRδ1$^{-/-}$ mouse cochlear sections.

Cochlear responses. Given the strong cochlear expression of GluRδ1, we examined cochlear function in GluRδ1$^{-/-}$ mice. The three assays used were (i) ABR, the summed sound-evoked activity of the auditory nerve and ascending auditory neural pathways; (ii) DPOAE, a sound-evoked preneural signal generated and amplified by the OHCs and transmitted back to the ear canal; and (iii) the magnitude of the EP, the potential generated by the stria vascularis and measured inside the endolymphatic space, which generates the transepithelial electric driving force necessary to drive transduction currents through the hair cell stereocilia when they are deflected by acoustic stimulation.

At 6 to 8 weeks of age, ABR thresholds in GluRδ1$^{-/-}$ mice were elevated compared with those in GluRδ1$^{+/+}$ mice by 20 to 45 dB for frequencies of >16 kHz (Fig. 3A) (differences between GluRδ1$^{+/+}$ and GluRδ1$^{-/-}$ mice were significant by two-way ANOVA; $P = 0.003$; $F = 21.77$). At lower frequencies (<16 kHz), threshold elevation was <10 dB. Thresholds in GluRδ1$^{+/-}$ mice were intermediate between those in GluRδ1$^{+/+}$ and GluRδ1$^{-/-}$ mice. DPOAEs showed similar patterns of threshold elevation (Fig. 3B): differences between GluRδ1$^{+/+}$ and GluRδ1$^{-/-}$ mice for test frequencies of >16 kHz were significant by two-way ANOVA ($P = 0.01$; $F = 10.43$). Suprathreshold ABR and DPOAE amplitudes were also significantly reduced in GluRδ1$^{-/-}$ mice at frequencies of >16 kHz (data not shown); however, there were no significant changes in response waveforms.

EP measured in the basal turn (Fig. 3C), a cochlear location corresponding to the 45-kHz tonotopic location (17), was lower in GluRδ1$^{-/-}$ mice (77.1 ± 8.2 mV [mean ± standard error of the mean {SEM}]; $n = 7$) than in GluRδ1$^{+/+}$ (100.7 ± 3.2 mV [mean ± SEM]; $n = 7$) and GluRδ1$^{+/-}$ mice (90.0 ± 6.2 mV [mean ± SEM]; $n = 7$). The difference between GluRδ1$^{-/-}$ and GluRδ1$^{+/+}$ mice was significant (P was <0.01 by Student's t test; P was <0.05 by one-way ANOVA).

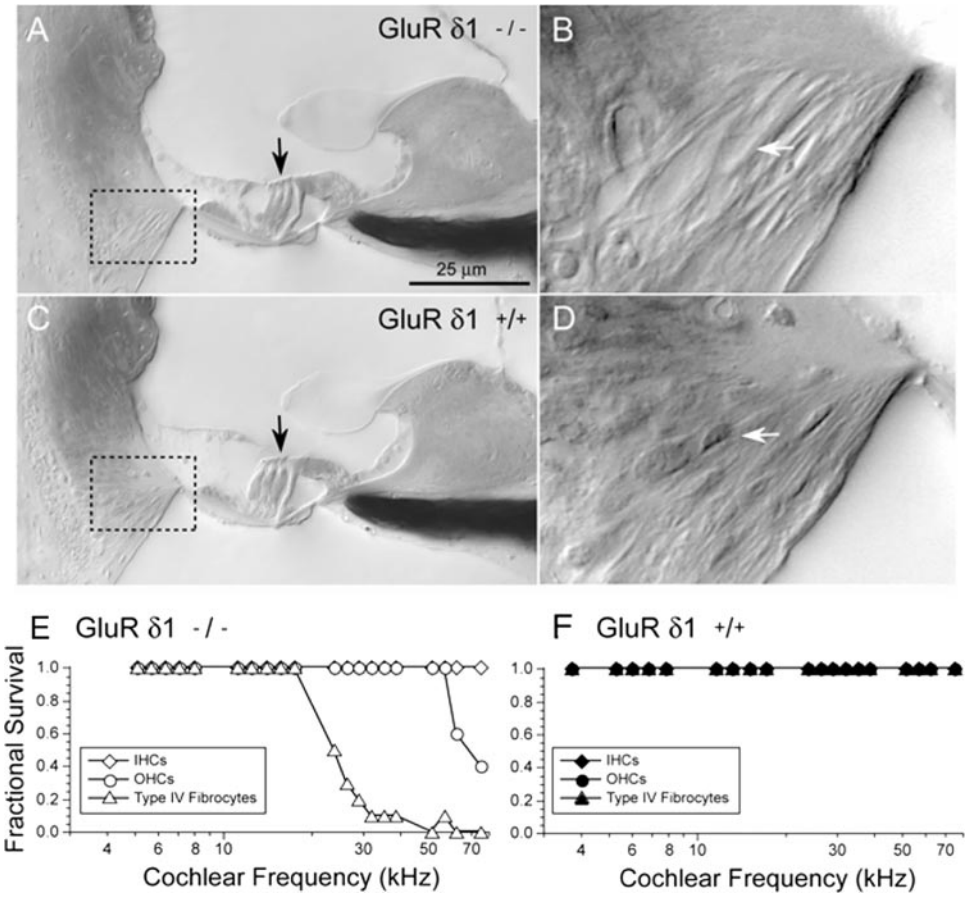

FIG. 4. There is a loss of type IV fibrocytes from the spiral ligaments in the high-frequency regions of ears of GluRδ1$^{-/-}$ mice. Panels A and C show place-matched views of the upper basal turn (~30-kHz region) from an ear of a GluRδ1$^{-/-}$ mouse and an ear of a GluRδ1$^{+/+}$ mouse, respectively. Arrows point to OHCs; dotted boxes show the region of the spiral ligament where type IV fibrocytes are normally found. Panels B and D enlarge these regions. The white arrow in panel D indicates the nucleus of a type IV fibrocyte in the ear of the GluRδ1$^{+/+}$ mouse; the arrow in panel B shows the absence of this cell type in the ear of the GluRδ1$^{-/-}$ mouse, which leaves characteristic gaps in the extracellular matrix. Panels E and F show the estimated fractional survival of IHCs, OHCs, and type IV fibrocytes in an ear of a GluRδ1$^{-/-}$ mouse and an ear of a GluRδ1$^{+/+}$ mouse, respectively, as a function of cochlear location (converted to frequency).

Cochlear morphology and immunostaining. To evaluate morphological changes in the GluRδ1$^{-/-}$ mice, we examined plastic sections of osmium-stained cochleas. Histologic staining in GluRδ1$^{-/-}$ mice (8 weeks old) showed a pathological pattern consisting of variable and scattered OHC loss in the basalmost region of the cochlea (Fig. 4E) and consistent and substantial loss of type IV fibrocytes in the spiral ligament (Fig. 4D) throughout much of the basal turn (Fig. 4E). As shown in high-power micrographs (Fig. 4B and D), the nuclei of type IV fibrocytes are normally visible interspersed among a complex fibrous network visible in differential interference contrast optics (Fig. 4D). In the mutant, all cell nuclei are absent in this region of the spiral ligament, and only the fibrous network remains (Fig. 4B). According to a mouse cochlear frequency map (8), the OHC loss was restricted to cochlear frequency regions well above that where the threshold shift was seen; however, the region of spiral ligament pathology correlated well with the region of threshold shift. Quantitative results from one ear of each genotype are shown in Fig. 4E to F: similar results for the loss of fibrocytes were seen in the other ears evaluated ($n = 3$ of each genotype). There was no loss of IHCs or cochlear neurons, and all other structures of the cochlear duct, including the stria vascularis, appeared normal.

To further evaluate the condition of remaining cells of the spiral ligament and stria vascularis, we performed immunostaining for markers normally expressed in these areas and implicated in ionic homeostasis and therefore EP generation: Kv3.1b, Kir4.1, Atp1b1, and Nkcc1 (7, 10, 14, 38). There was little evidence of down-regulation of these key channels/pumps, except that Kv3.1b staining was reduced or absent in regions where type IV fibrocytes were missing in the basal turns but remained present in the type IV fibrocytes in the apical and middle turns and even in adjacent cells in the basal turns (Fig. 5A and B; data not shown). Similarly, Kir4.1 and Atp1b1 appeared normal in marginal cells of the stria vascularis (Fig. 5C, D, G, H). Kir4.1 expression also appeared normal in the Deiters' cells, the supporting cells for OHCs, in both GluRδ1$^{+/+}$ and GluRδ1$^{-/-}$ mice (data not shown). No significant change in Nkcc1 staining was observed in marginal cells, type IV fibrocytes, and other cochlear cells of GluRδ1$^{-/-}$ or GluRδ1$^{+/+}$ mice (Fig. 5E and F; data not shown).

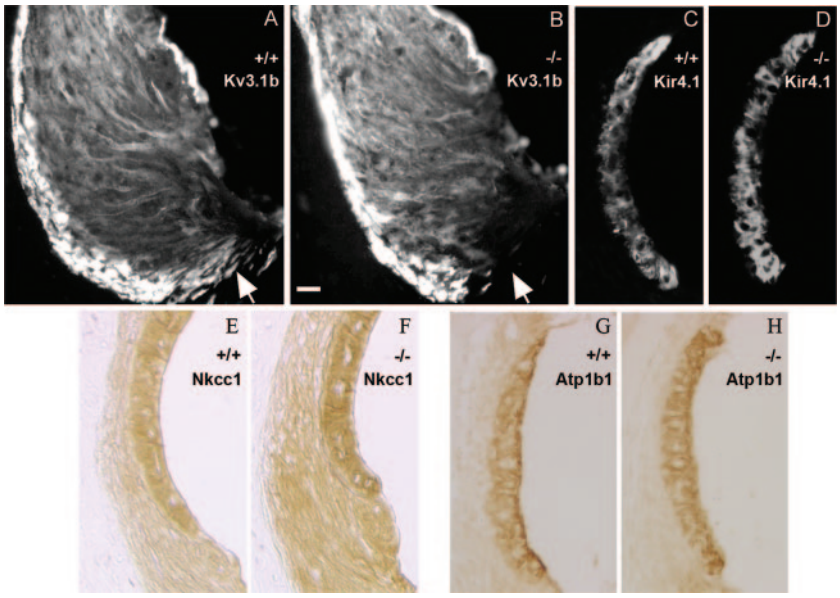

FIG. 5. Immunostaining of Kv3.1b (A and B) was reduced and lost in type IV fibrocytes (arrows) but normal in other fibrocytes of spiral ligament in the basal turn. Immunostaining of Kir4.1 (C and D), Nkcc1 (E and F), and Atp1b1 (G and H) appeared unaffected in marginal cells of stria vascularis. The bar in panel B (20 μm) applies to all panels. +/+, GluRδ1$^{+/+}$; −/−, GluRδ1$^{-/-}$.

Cochlear vulnerability to noise damage. Synaptic transmission between the IHC and its afferent innervation is glutamatergic, and acoustic overstimulation produces a type of glutamate excitotoxicity that can contribute to temporary noise-induced threshold shifts after acoustic overstimulation. In search of a functional role for the GluRδ1 receptor in the IHC area, we examined the vulnerability of GluRδ1$^{-/-}$ mice to temporary acoustic injury. Twelve hours after a 2-h exposure to a noise band (8 to 16 kHz) at 89 dB SPL, GluRδ1$^{+/+}$ mice displayed threshold shifts in both ABR (Fig. 6A) and DPOAE (Fig. 6B) responses that recovered within 1 week (data not shown). In GluRδ1$^{-/-}$ mice, the temporary threshold shift was much larger for the same exposure, and the increased dysfunction was seen in both ABR and DPOAE (Fig. 6A and B). The symmetry of the threshold shifts in both the neural (ABR) and the preneural, OHC-based measures (DPOAE) suggests that the shifts are well explained by OHC dysfunction and, thus, that the increased vulnerability did not arise exclusively in the IHC area, i.e., it is not due to enhanced excitotoxicity at the IHC/afferent synapse (29). In contrast, when the efferent innervation of the IHCs is selectively destroyed, the increased vulnerability is seen only in the ABRs and not the DPOAEs, consistent with changes in synaptic transmission associated with excitotoxicity (5).

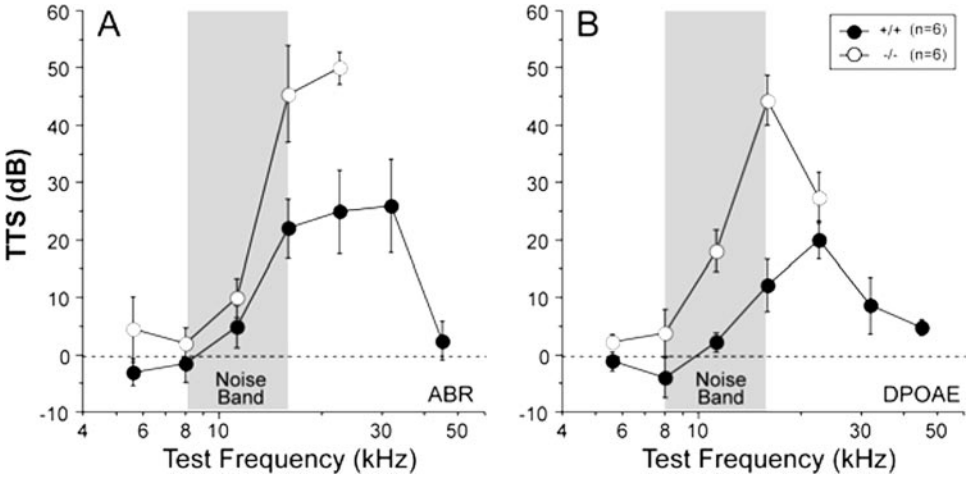

FIG. 6. GluRδ1$^{-/-}$ (−/−) mice are more vulnerable to acoustic injury. Temporary threshold shifts were measured in both ABR (A) and DPOAE (B) 12 h after exposure to an octave band noise at 8 to 16 kHz at 89 dB SPL for 2 h. Means and standard errors (error bars) are shown; numbers of animals in each group are in the key in panel B, which applies to both panels. Threshold shifts are not shown for the two highest test frequencies because some of the GluRδ1$^{-/-}$ mice showed preexposure thresholds at or near the sound pressure ceiling of our functional assay. +/+, GluRδ1$^{+/+}$.

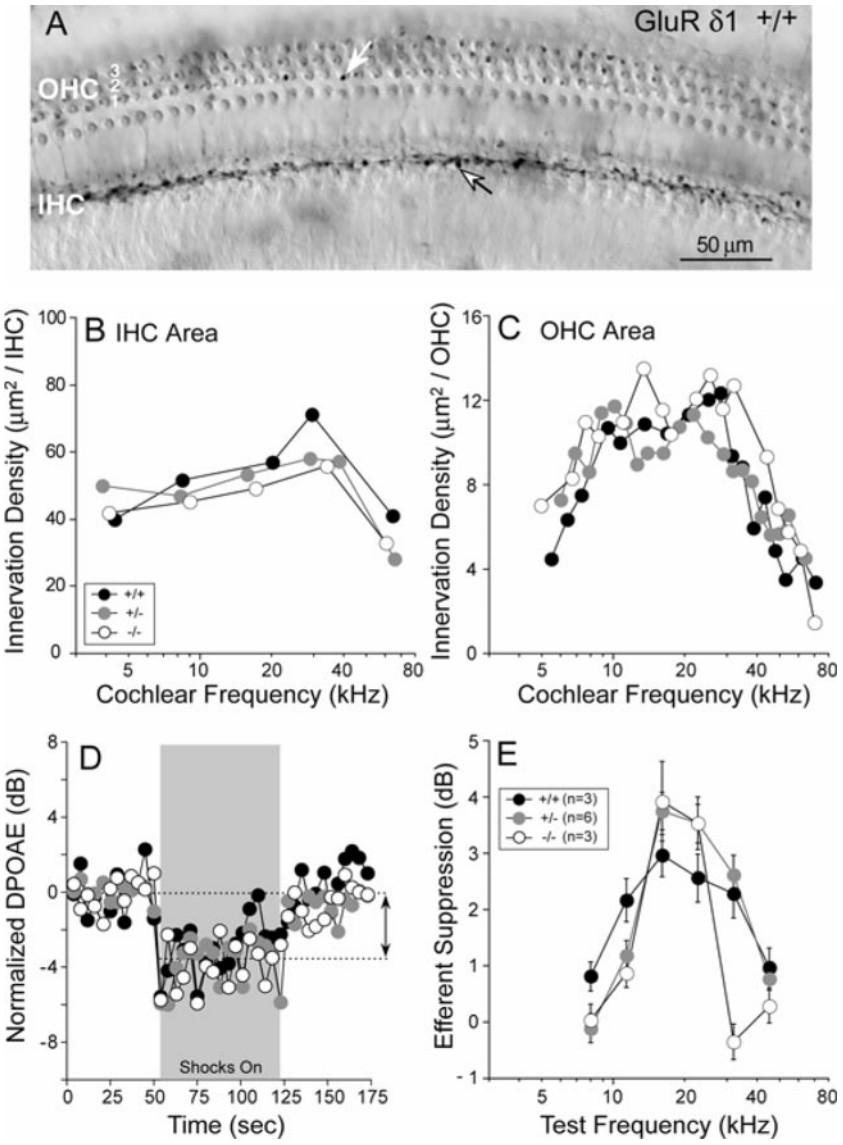

FIG. 7. There is no change in the density of efferent innervation (A to C) or in the strength of shock-evoked efferent effects (D and E) in GluRδ1$^{-/-}$ mice. Panel A shows SNAP25 immunostained efferent terminals in the ear of a GluRδ1$^{+/+}$ mouse. The white arrow marks a terminal in the OHC area, the black-rimmed arrow shows a terminal in the IHC area. Panels B and C show the total silhouette area of immunostained terminals as a function of cochlear location (converted to frequency) in one ear from each genotype. In the OHC area (C), values are averaged over all three OHC rows. Panel D shows representative data for each genotype from the assay used to measure cochlear efferent suppression. DPOAE amplitude (evoked with f_2 at 16 kHz) was measured repeatedly before, during, and after a train of shocks to the efferent bundle; efferent suppression of DPOAE amplitude (the difference between the two dashed lines) was measured. Panel E shows average values of efferent suppression at different test frequencies obtained from a cohort of animals using the assay illustrated in panel D. Means and standard errors (error bars) are shown. +/+, GluRδ1$^{+/+}$; −/−, GluRδ1$^{-/-}$; +/−, GluRδ1$^{+/-}$.

Cochlear efferent innervation and efferent inhibition. The vulnerability of the cochlea to acoustic injury is controlled, in part, by a cholinergic feedback inhibitory circuit to the OHCs, the medial olivocochlear pathway (27). Given the enhanced vulnerability of the GluRδ1$^{-/-}$ mice to acoustic injury, we evaluated the integrity of the efferent innervation, both morphologically and functionally.

To assess the density of efferent innervation, we immunostained cochlear whole mounts for SNAP25 (Fig. 7A) or synaptophysin (synaptic vesicle-associated proteins abundant in efferent terminals) or CGRP or VAT (markers for neurotransmitters found in efferent terminals; data not shown). Qualitative analysis suggested no abnormalities in the efferent innervation of the GluRδ1$^{-/-}$ ears. In one cochlea from each genotype, we quantified SNAP25 immunostaining in both IHC and OHC areas and found no significant differences (Fig. 7B and C).

To assess the function of the OHC efferent pathway, we measured the suppression of the DPOAEs elicited by electrical stimulation of the efferent bundle at the floor of the IVth ventricle (Fig. 7D). There were no significant differences among the three genotypes in the mean magnitude of this

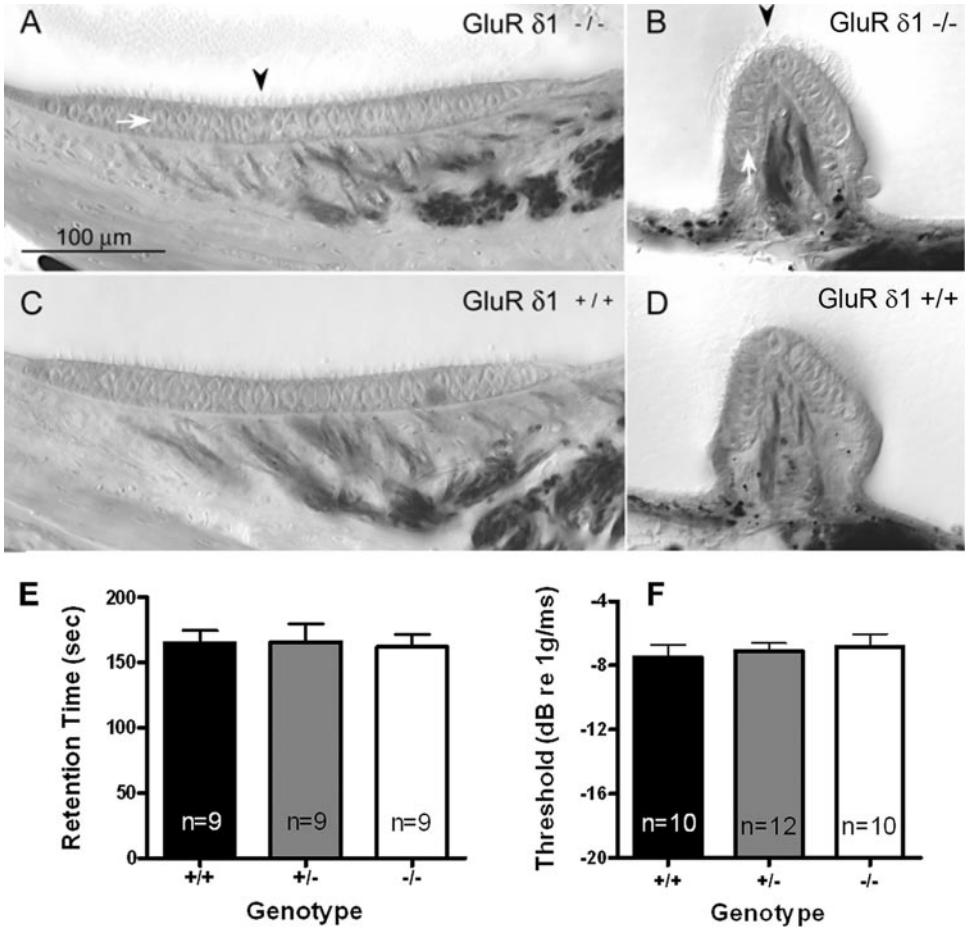

FIG. 8. GluRδ1$^{-/-}$ mice display normal vestibular sensory epithelial morphology and function. Micrographs are from the saccular macula (A and C) and the posterior canal ampulla (B and D) of mice at 2 months of age. White arrows point to hair cell bodies; black arrowheads point to hair bundles. The scale bar in panel A applies to panels A through D. (E) The retention time (mean and SEM [error bars]) in the Rotarod test did not reveal significant differences among mice of three genotypes at 2 months of age. The number of mice tested in each group is illustrated. (F) Threshold measurements (mean and SEM [error bars]) of linear VsEPs did not show significant differences among mice of three genotypes at ages of between 2 and 3 months. The stimulus amplitude was described in dB re: 1.0g/ms and ranged from −18 to + 6 dB re: 1.0g/ms, adjusted in 3-dB steps. The number of mice tested in each group is illustrated. +/+, GluRδ1$^{+/+}$; −/−, GluRδ1$^{-/-}$; +/−, GluRδ1$^{+/-}$.

efferent effect (Fig. 7E), except at 32 kHz, where the reduced efferent effect in the GluRδ1$^{-/-}$ mice is well explained by the OHC dysfunction in that region, as seen by the threshold elevation in both ABRs and DPOAEs (Fig. 3A and B). Since the efferent suppressive effect on cochlear sound-induced vibration arises by reducing the OHCs' contribution to cochlear amplification, efferent effect size is always reduced in areas of OHC dysfunction. We conclude that the deletion of GluRδ1 did not affect efferent synaptic transmission and that efferent dysfunction cannot account for the enhanced vulnerability to acoustic injury.

Vestibular morphology and function. The presence of GluRδ1 in vestibular hair cells (both type I and type II) and vestibular ganglia (36) suggested a role in vestibular function. We first analyzed morphology of vestibular end organs in osmicated plastic sections and hematoxylin-and-eosin-stained paraffin sections (see Materials and Methods). There were no changes in morphology of the saccule, utricle, or semicircular canals or in their afferent innervation in the GluRδ1$^{-/-}$ mice (Fig. 8A to D; data not shown). Vestibular function was measured at 2 months, both behaviorally (Rotarod and swim tests) and electrophysiologically (VsEP, the summed neural activity of vestibular afferents from the utricle and saccule, and the ascending vestibular pathway, evoked by linear acceleration stimuli). The loss of GluRδ1 had no significant effect on the ability of mice to remain on a rotating rod as its speed of revolution increased (Fig. 8E) or on the time required to right themselves and begin swimming after being dropped into a water bath (data not shown). On average, VsEP thresholds were slightly higher in GluRδ1$^{-/-}$ mice than in GluRδ1$^{+/+}$ mice. However, differences among the groups were not statistically significant (ANOVA) (Fig. 8F). Similarly, P1 peak latency, P2 peak latency, P1-N1 amplitudes, and P2-N2 amplitudes were not significantly different among the three genotypes (multivariate ANOVA). All response parameters were similar to normative values in normal young and adult mice (18, 19). These data suggest that the absence of the GluRδ1 does not significantly alter gravity receptor function or balance behavior.

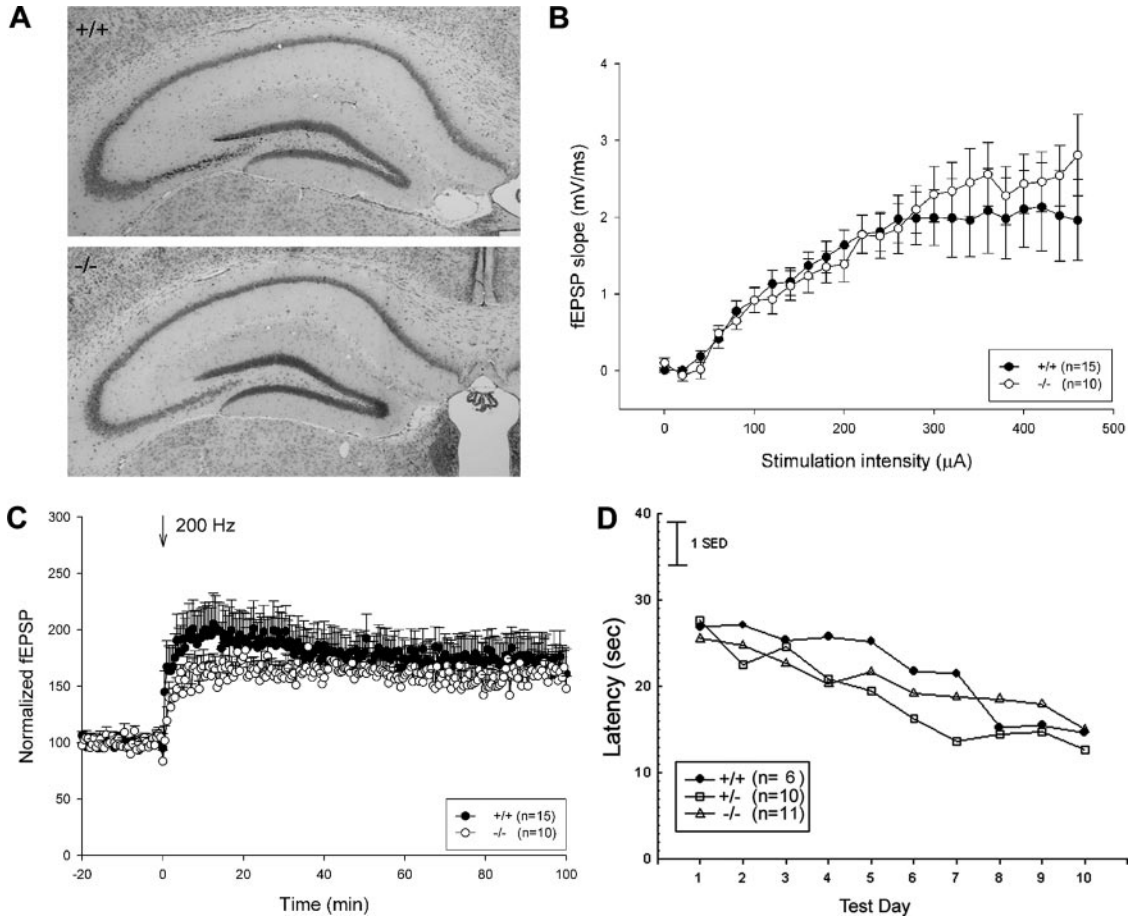

FIG. 9. Hippocampal morphology and function appear normal in GluRδ1$^{-/-}$ mice. (A) Hematoxylin and eosin staining of hippocampi in GluRδ1$^{+/+}$ (+/+) and GluRδ1$^{-/-}$ (−/−) mice at 2 months old. No obvious differences in neuronal location, number, and position were detected between the hippocampuses of GluRδ1$^{+/+}$ and GluRδ1$^{-/-}$ mice. Synaptic transmission appeared normal in hippocampal slices of GluRδ1$^{+/+}$ and GluRδ1$^{-/-}$ mice at 2 months old (B and C). (B) Recordings of the extracellular fEPSPs showed that the loss of GluRδ1 did not cause any significant changes in synaptic transmission over a wide range of stimulus intensities. (C) A 200-Hz tetanic stimulation enhanced the fEPSPs to 159 ± 13% (mean ± SEM [error bars]; $n = 10$) and 174 ± 17% ($n = 15$; P was >0.05 by the Kolmogorov-Smirnov test) of their initial levels, when measured 60 min after tetanization in slices from GluRδ1$^{-/-}$ and GluRδ1$^{+/+}$ mice, respectively. (D) Performance in the place task of the water maze did not show significant differences among GluRδ1$^{+/+}$, GluRδ1$^{+/-}$ (+/−), and GluRδ1$^{-/-}$ mice at 2 to 3 months of age ($n = 6$, 10, 11, respectively). Mean latency to reach the hidden platform is shown on each of the 10 test days. All groups performed similarly in this task. The vertical bar indicates one standard error of the difference (SED) in group means.

Hippocampal morphology and function. Because of the high level of GluRδ1 mRNA and protein in adult hippocampus (Fig. 2B) (25, 36), we compared hippocampal morphology and synaptic function in GluRδ1$^{+/+}$ and GluRδ1$^{-/-}$ mice at 2 months of age. As shown in Fig. 9A, no gross morphological differences were detected among the genotypes. Because the deletion of GluRδ2 strongly affects long-term depression of synaptic transmission in the cerebellum, we examined the role of GluRδ1 in synaptic transmission and synaptic plasticity at excitatory synapses between CA3 and CA1 pyramidal neurons (CA3-CA1 synapses) in hippocampal slices (Fig. 9B and C). Recordings of the extracellular fEPSP showed that the loss of GluRδ1 did not cause any significant changes in synaptic transmission (Fig. 9B). Thus, input-output curves recorded over a wide range of stimulus intensities were normal in GluRδ1$^{-/-}$ mice compared to their GluRδ1$^{+/+}$ littermates. We next explored the effect of GluRδ1 deficiency on LTP at CA3-CA1 synapses. We chose a 200-Hz stimulation protocol that induced a compound LTP that consisted of both presynaptic and postsynaptic modules of LTP expression (47). We found no significant changes in compound LTP between GluRδ1$^{+/+}$ and GluRδ1$^{-/-}$ mice (Fig. 9C). Thus, the 200-Hz tetanic stimulation fEPSPs was increased to 159 ± 13% of initial levels in slices from GluRδ1$^{-/-}$ mice (mean ± SEM; $n = 10$) and 174 ± 17% in GluRδ1$^{+/+}$ mice ($n = 15$; P was >0.05 by the Kolmogorov-Smirnov test) 60 min after tetanization. Similarly, fEPSPs measured at 10 or 90 min after 200-Hz tetanization were not significantly different in GluRδ1$^{-/-}$ mice compared to those in their GluRδ1$^{+/+}$ littermates (P was >0.05 by the Kolmogorov-Smirnov test). The Morris water maze was used to test hippocampal function in vivo. As shown in Fig. 9D, mice of all genotypes learned the task as indicated by the steady decline in latency to find the hidden platform (ANOVA; day; $F = 20.25$, df = 9,216, $P < 0.001$). There were no significant group differences in the

acquisition of this task (ANOVA; group × day; $F = 1.33$, $df = 18,216$; $P > 0.05$).

DISCUSSION

Targeted disruption of GluRδ1 causes significant hearing loss at high frequencies, associated with reductions of both OHC function and EP, the resting potential of the lumen of the cochlear duct that helps drive receptor currents into sensory cells. These findings provide the first in vivo evidence of a functional role for this largely uncharacterized orphan glutamate receptor, which is consistent with its prominent inner ear expression. Given the prevalence of congenital or acquired high-frequency hearing loss in human ears, the locus encoding GluRδ1 represents a candidate disease gene (39).

In contrast, the apparently normal function and morphology in vestibular sensory-end organs and hippocampus in GluRδ1$^{-/-}$ mice suggest that functional redundancy exists for the GluRδ1 expressed in these areas. Given the lack of other members of the GluRδ family in human and mouse genome sequences, it is conceivable that other proteins with little sequence homology to GluRδ1 may compensate for the lack of GluRδ1 in vestibular end organs and hippocampus.

Cochlear dysfunction and EP reduction. The high-frequency threshold elevation observed in the GluRδ1$^{-/-}$ mice was on the order of 20 to 45 dB as measured in the neural response (ABR) and roughly half that as measured in the preneural response (DPOAE). This hearing loss was associated with a reduction in the EP of 20 to 25 mV, as measured in the basal turn at roughly the 45-kHz place. A number of lines of evidence converge to suggest that both the pattern and degree of threshold elevations are well explained qualitatively and quantitatively by the EP reduction (29), i.e., there is no reason to assume dysfunction in the sensory cells and nerve fibers per se.

Decreasing the EP reduces the driving force for sound-elicited transduction currents into both IHCs and OHCs. This reduction seen by the OHCs reduces their somatic electromotility and thereby decreases mechanical motions of the cochlear partition and elevates thresholds as seen by both DPOAEs and ABRs (35). Threshold elevation in cochlear neurons is further increased by effects at the IHCs, since these IHCs provide exclusive synaptic drive to 95% of these nerve fibers. The EP reduction seen by IHCs reduces the receptor potentials which drive synaptic transmission, even without a change in cochlear vibration. Thus, cochlear dysfunction from EP reduction results in larger changes in ABR (neural) thresholds than in DPOAE thresholds (which require only normal OHC function). Indeed a recent empirical comparison of ABR shifts and DPOAE shifts in furosemide-treated gerbils showed a ratio very similar to that seen here (29).

According to studies of click-evoked neural potentials in cats, there is roughly a 1-dB threshold shift in ABR for each 1-mV decrement in EP (37). Given that click-evoked thresholds in cat are dominated by midfrequency (5 to 10 kHz) neurons (1) and that the OHC contribution to the cochlear amplifier increases with frequency, it is not unlikely that, in the 16- to 45-kHz region of the mouse, the relationship between neural thresholds and EP reduction is greater than 1 dB/mV. Thus, the ABR and DPOAE shifts seen in the present study are well explained by the magnitude of the EP shift.

EP reduction and loss of spiral ligament cells. The EP is generated by coordinated ion pumping activity of numerous cell types in the spiral ligament and the stria vascularis. Numerous other deafness mutations appear to affect hearing via their effects on EP and cochlear ion homeostasis. Mutations in Cx26, Claudin-11, Pendrin, Claudin-14, Nkcc1, Kcc4, and various channels (e.g., Kir4.1 and Isk) can cause EP reduction and corresponding elevation of cochlear thresholds (2–4, 7, 11, 12, 22, 28, 41). Mice lacking Pou3f4, a transcription factor expressed in spiral ligament fibrocytes, showed a 50-mV EP reduction associated with a 70- to 80-dB elevation of ABR thresholds. Interestingly, such a profound cochlear dysfunction (much more dramatic than that seen here with the loss of GluRδ1) was associated with very subtle morphological changes. Hair cells and the rest of the organ of Corti were normal in Pou3f4 mice, with ultrastructural changes noted only in spiral ligament fibrocytes (type I and type II) (30). Mice lacking otospiralin, a protein of unknown function produced by spiral ligament fibrocytes, displayed modest threshold elevation (20 dB by ABR) associated with subtle changes in morphology of type II and type IV fibrocytes, visible only at the ultrastructural level. EP was not measured in this mutant line (6).

Type IV fibrocytes in GluRδ1$^{-/-}$ mice were eliminated throughout the basal turn. However, this fibrocyte loss was probably not the cause of the EP reduction. Acoustic overstimulation experiments in mice have shown that type IV fibrocytes, among the most vulnerable cells in the ear, can be eliminated after moderate noise exposures, yet ABR thresholds and EP values can completely recover (17, 42). Similarly, in a mouse (C57BL/6) with progressive, high-frequency age-related hearing loss, type IV fibrocytes are also among the first cells to disappear from the basal turn (13) and, although high-frequency thresholds are elevated, the EP is not reduced (23, 31) (K. Hirose and M. C. Liberman, unpublished data).

Given that GluRδ1 was expressed in IHCs, OHCs, and spiral ganglion neurons but not in the spiral ligament, possible explanations for the EP shifts based on cellular changes outside the stria and ligament must be considered. One possible link is that the generation of a normal EP must depend on appropriate recycling of K^+ from the hair cells to the stria via the spiral ligament (43), and the loss of GluRδ1 may disrupt that recycling in either the IHC or the OHC areas. The organ of Corti is both mechanically labile and "leaky" to ion flux, as a result of the effects of the loss of GluRδ1 on one or more supporting cells. Direct measurement of the input impedance of scala media may address this issue, although such an approach is tedious and artifact prone.

Glutamatergic transmission and loss of OHC function. Although there is a rich efferent innervation of hair cells and cochlear neurons, there is no evidence for glutamatergic synapses in the efferent system; correspondingly, our findings showed no effects of GluRδ1 deletion on efferent innervation or the strength of efferent-evoked effects on cochlear response (i.e., DPOAEs). However, the striking increase in vulnerability of the ears of GluRδ1$^{-/-}$ mice to temporary acoustic injury seen in this study was consistent with a role of GluRδ1 in OHCs. In particular, the similarity in noise-induced DPOAE shifts and ABR shifts suggests that increased vulnerability is occurring presynaptically, e.g., involving OHCs and their role as cochlear amplifiers. The presence of GluRδ1 in OHCs in

our study and others (36) is consistent with such a notion. The afferent synapse between OHCs and type II cochlear nerve fibers is poorly understood. It is not clear whether afferent transmission there is glutamatergic (33, 34); glutamate excitotoxicity is not seen in the OHC area after acoustic overstimulation (33, 34), and the efferent synapses on OHCs are clearly cholinergic in nature with end effects mediated via the α9/α10 nicotinic acetylcholine receptors (9, 40). Thus, it is difficult to propose a compelling argument as to why GluRδ1 loss should enhance damage to OHCs per se. An alternate hypothesis is that the heightened vulnerability arises via increased fragility of the EP generation mechanisms such that the increased demands on the system imposed during acoustic overstimulation lead to further EP reductions not seen in mice with more robust ion homeostasis.

ACKNOWLEDGMENTS

We thank M. Li and T. Yamashita for assistance and R. Smeyne, C. Faherty, M. Yuzaki, T. Curran, and C. Brumwell for advice. We also thank M. Yuzaki and R. Wenthold for generously providing GluRδ1/2 and GluRδ1 antibodies.

This work was supported in part by Public Health Service grants DC06471, DC05168, DC04761, DC0188, DC04477, and DC05761; Cancer Center core grant CA21765; and NIDCD core grant P30 DC05209 from the National Institutes of Health; the Royal National Institute for the Deaf; the American Lebanese Syrian Associated Charities; the Basil O'Connor Starter Scholar Research Award 5-FY98-0725 from the March of Dimes Birth Defects Foundation; the NARSAD Young Investigator Award; and the Whitehall Foundation.

REFERENCES

1. **Antoli-Candela, F. J., and N. Y. S. Kiang.** 1978. Unit activity underlying the N1 potential, p. 165–191. *In* R. F. Naunton and C. Fernández (ed.), Evoked electrical activity in the auditory nervous system. Academic Press, New York, NY.
2. **Ben-Yosef, T., I. A. Belyantseva, T. L. Saunders, E. D. Hughes, K. Kawamoto, C. M. Van Itallie, L. A. Beyer, K. Halsey, D. J. Gardner, E. R. Wilcox, J. Rasmussen, J. M. Anderson, D. F. Dolan, A. Forge, Y. Raphael, S. A. Camper, and T. B. Friedman.** 2003. Claudin 14 knockout mice, a model for autosomal recessive deafness DFNB29, are deaf due to cochlear hair cell degeneration. Hum. Mol. Genet. **12:**2049–2061.
3. **Boettger, T., C. A. Hubner, H. Maier, M. B. Rust, F. X. Beck, and T. J. Jentsch.** 2002. Deafness and renal tubular acidosis in mice lacking the K-Cl co-transporter Kcc4. Nature **416:**874–878.
4. **Cohen-Salmon, M., T. Ott, V. Michel, J. P. Hardelin, I. Perfettini, M. Eybalin, T. Wu, D. C. Marcus, P. Wangemann, K. Willecke, and C. Petit.** 2002. Targeted ablation of connexin26 in the inner ear epithelial gap junction network causes hearing impairment and cell death. Curr. Biol. **12:**1106–1111.
5. **Darrow, K. N., S. F. Maison, and M. C. Liberman.** 2007. Selective removal of lateral olivocochlear efferents increases vulnerability to acute acoustic injury. J. Neurophysiol. **97:**1775–1785.
6. **Delprat, B., J. Ruel, M. J. Guitton, G. Hamard, M. Lenoir, R. Pujol, J. L. Puel, P. Brabet, and C. P. Hamel.** 2005. Deafness and cochlear fibrocyte alterations in mice deficient for the inner ear protein otospiralin. Mol. Cell. Biol. **25:**847–853.
7. **Dixon, M. J., J. Gazzard, S. S. Chaudhry, N. Sampson, B. A. Schulte, and K. P. Steel.** 1999. Mutation of the Na-K-Cl co-transporter gene Slc12a2 results in deafness in mice. Hum. Mol. Genet. **8:**1579–1584.
8. **Ehret, G.** 1983. Peripheral anatomy and physiology II, p. 169–200. *In* J. F. Willott (ed.), The auditory psychobiology of the mouse. Charles C. Thomas, Springfield, IL.
9. **Elgoyhen, A. B., D. E. Vetter, E. Katz, C. V. Rothlin, S. F. Heinemann, and J. Boulter.** 2001. alpha10: a determinant of nicotinic cholinergic receptor function in mammalian vestibular and cochlear mechanosensory hair cells. Proc. Natl. Acad. Sci. USA **98:**3501–3506.
10. **Erichsen, S., J. Zuo, L. Curtis, K. Rarey, and M. Hultcrantz.** 1996. Na,K-ATPase alpha- and beta-isoforms in the developing cochlea of the mouse. Hear. Res. **100:**143–149.
11. **Everett, L. A., I. A. Belyantseva, K. Noben-Trauth, R. Cantos, A. Chen, S. I. Thakkar, S. L. Hoogstraten-Miller, B. Kachar, D. K. Wu, and E. D. Green.** 2001. Targeted disruption of mouse Pds provides insight about the inner-ear defects encountered in Pendred syndrome. Hum. Mol. Genet. **10:**153–161.
12. **Gow, A., C. Davies, C. M. Southwood, G. Frolenkov, M. Chrustowski, L. Ng, D. Yamauchi, D. C. Marcus, and B. Kachar.** 2004. Deafness in Claudin 11-null mice reveals the critical contribution of basal cell tight junctions to stria vascularis function. J. Neurosci. **24:**7051–7062.
13. **Hequembourg, S., and M. C. Liberman.** 2001. Spiral ligament pathology: a major aspect of age-related cochlear degeneration in C57BL/6 mice. J. Assoc. Res. Otolaryngol. **2:**118–129.
14. **Hibino, H., Y. Horio, A. Inanobe, K. Doi, M. Ito, M. Yamada, T. Gotow, Y. Uchiyama, M. Kawamura, T. Kubo, and Y. Kurachi.** 1997. An ATP-dependent inwardly rectifying potassium channel, KAB-2 (Kir4. 1), in cochlear stria vascularis of inner ear: its specific subcellular localization and correlation with the formation of endocochlear potential. J. Neurosci. **17:**4711–4721.
15. **Hirai, H., T. Launey, S. Mikawa, T. Torashima, D. Yanagihara, T. Kasaura, A. Miyamoto, and M. Yuzaki.** 2003. New role of δ2-glutamate receptors in AMPA receptor trafficking and cerebellar function. Nat. Neurosci. **6:**869–876.
16. **Hirai, H., Z. Pang, D. Bao, T. Miyazaki, L. Li, E. Miura, J. Parris, Y. Rong, M. Watanabe, M. Yuzaki, and J. I. Morgan.** 2005. Cbln1 is essential for synaptic integrity and plasticity in the cerebellum. Nat. Neurosci. **8:**1534–1541.
17. **Hirose, K., and M. C. Liberman.** 2003. Lateral wall histopathology and endocochlear potential in the noise-damaged mouse cochlea. J. Assoc. Res. Otolaryngol. **4:**339–352.
18. **Jones, S. M., G. Subramanian, W. Avniel, Y. Guo, R. F. Burkard, and T. A. Jones.** 2002. Stimulus and recording variables and their effects on mammalian vestibular evoked potentials. J. Neurosci. Methods **118:**23–31.
19. **Jones, T. A., and S. M. Jones.** 1999. Short latency compound action potentials from mammalian gravity receptor organs. Hear. Res. **136:**75–85.
20. **Kashiwabuchi, N., K. Ikeda, K. Araki, T. Hirano, K. Shibuki, C. Takayama, Y. Inoue, T. Kutsuwada, T. Yagi, Y. Kang, et al.** 1995. Impairment of motor coordination, Purkinje cell synapse formation, and cerebellar long-term depression in GluR δ2 mutant mice. Cell **81:**245–252.
21. **Kohda, K., Y. Wang, and M. Yuzaki.** 2000. Mutation of a glutamate receptor motif reveals its role in gating and δ2 receptor channel properties. Nat. Neurosci. **3:**315–322.
22. **Kudo, T., S. Kure, K. Ikeda, A. P. Xia, Y. Katori, M. Suzuki, K. Kojima, A. Ichinohe, Y. Suzuki, Y. Aoki, T. Kobayashi, and Y. Matsubara.** 2003. Transgenic expression of a dominant-negative connexin26 causes degeneration of the organ of Corti and non-syndromic deafness. Hum. Mol. Genet. **12:**995–1004.
23. **Lang, H., B. A. Schulte, and R. A. Schmiedt.** 2002. Endocochlear potentials and compound action potential recovery: functions in the C57BL/6J mouse. Hear. Res. **172:**118–126.
24. **Lein, E. S., M. J. Hawrylycz, N. Ao, M. Ayres, A. Bensinger, A. Bernard, A. F. Boe, M. S. Boguski, K. S. Brockway, E. J. Byrnes, L. Chen, L. Chen, T. M. Chen, M. C. Chin, J. Chong, B. E. Crook, A. Czaplinska, C. N. Dang, S. Datta, N. R. Dee, A. L. Desaki, T. Desta, E. Diep, T. A. Dolbeare, M. J. Donelan, H. W. Dong, J. G. Dougherty, B. J. Duncan, A. J. Ebbert, G. Eichele, L. K. Estin, C. Faber, B. A. Facer, R. Fields, S. R. Fischer, T. P. Fliss, C. Frensley, S. N. Gates, K. J. Glattfelder, K. R. Halverson, M. R. Hart, J. G. Hohmann, M. P. Howell, D. P. Jeung, R. A. Johnson, P. T. Karr, R. Kawal, J. M. Kidney, R. H. Knapik, C. L. Kuan, J. H. Lake, A. R. Laramee, K. D. Larsen, C. Lau, T. A. Lemon, A. J. Liang, Y. Liu, L. T. Luong, J. Michaels, J. J. Morgan, R. J. Morgan, M. T. Mortrud, N. F. Mosqueda, L. L. Ng, R. Ng, G. J. Orta, C. C. Overly, T. H. Pak, S. E. Parry, S. D. Pathak, O. C. Pearson, R. B. Puchalski, Z. L. Riley, H. R. Rockett, S. A. Rowland, J. J. Royall, M. J. Ruiz, N. R. Sarno, K. Schaffnit, N. V. Shapovalova, T. Sivisay, C. R. Slaughterbeck, S. C. Smith, K. A. Smith, B. I. Smith, A. J. Sodt, N. N. Stewart, K. R. Stumpf, S. M. Sunkin, M. Sutram, A. Tam, C. D. Teemer, C. Thaller, C. L. Thompson, L. R. Varnam, A. Visel, R. M. Whitlock, P. E. Wohnoutka, C. K. Wolkey, V. Y. Wong, et al.** 2007. Genome-wide atlas of gene expression in the adult mouse brain. Nature **445:**168–176.
25. **Lomeli, H., R. Sprengel, D. J. Laurie, G. Kohr, A. Herb, P. H. Seeburg, and W. Wisden.** 1993. The rat delta-1 and delta-2 subunits extend the excitatory amino acid receptor family. FEBS Lett. **315:**318–322.
26. **Magdaleno, S., P. Jensen, C. L. Brumwell, A. Seal, K. Lehman, A. Asbury, T. Cheung, T. Cornelius, D. M. Batten, C. Eden, S. M. Norland, D. S. Rice, N. Dosooye, S. Shakya, P. Mehta, and T. Curran.** 2006. BGEM: an in situ hybridization database of gene expression in the embryonic and adult mouse nervous system. PLoS Biol. **4:**e86.
27. **Maison, S. F., A. E. Luebke, M. C. Liberman, and J. Zuo.** 2002. Efferent protection from acoustic injury is mediated via alpha9 nicotinic acetylcholine receptors on outer hair cells. J. Neurosci. **22:**10838–10846.
28. **Marcus, D. C., T. Wu, P. Wangemann, and P. Kofuji.** 2002. KCNJ10 (Kir4.1) potassium channel knockout abolishes endocochlear potential. Am. J. Physiol. Cell Physiol. **282:**C403–C407.
29. **Mills, D. M.** 2003. Differential responses to acoustic damage and furosemide in auditory brainstem and otoacoustic emission measures. J. Acoust. Soc. Am. **113:**914–924.
30. **Minowa, O., K. Ikeda, Y. Sugitani, T. Oshima, S. Nakai, Y. Katori, M. Suzuki, M. Furukawa, T. Kawase, Y. Zheng, M. Ogura, Y. Asada, K. Watanabe, H.**

Yamanaka, S. Gotoh, M. Nishi-Takeshima, T. Sugimoto, T. Kikuchi, T. Takasaka, and T. Noda. 1999. Altered cochlear fibrocytes in a mouse model of DFN3 nonsyndromic deafness. Science **285:**1408–1411.

31. **Ohlemiller, K. K., J. S. Wright, and A. F. Heidbreder.** 2000. Vulnerability to noise-induced hearing loss in 'middle-aged' and young adult mice: a dose-response approach in CBA, C57BL, and BALB inbred strains. Hear. Res. **149:**239–247.
32. **Pagedar, N. A., W. Wang, D. H. Chen, R. R. Davis, I. Lopez, C. G. Wright, and K. N. Alagramam.** 2006. Gene expression analysis of distinct populations of cells isolated from mouse and human inner ear FFPE tissue using laser capture microdissection—a technical report based on preliminary findings. Brain Res. **1091:**289–299.
33. **Puel, J. L., R. Pujol, F. Tribillac, S. Ladrech, and M. Eybalin.** 1994. Excitatory amino acid antagonists protect cochlear auditory neurons from excitotoxicity. J. Comp. Neurol. **341:**241–256.
34. **Ruel, J., R. P. Bobbin, D. Vidal, R. Pujol, and J. L. Puel.** 2000. The selective AMPA receptor antagonist GYKI 53784 blocks action potential generation and excitotoxicity in the guinea pig cochlea. Neuropharmacology **39:**1959–1973.
35. **Ruggero, M. A., and N. C. Rich.** 1991. Furosemide alters organ of Corti mechanics: evidence for feedback of outer hair cells upon the basilar membrane. J. Neurosci. **11:**1057–1067.
36. **Safieddine, S., and R. J. Wenthold.** 1997. The glutamate receptor subunit δ1 is highly expressed in hair cells of the auditory and vestibular systems. J. Neurosci. **17:**7523–7531.
37. **Sewell, W. F.** 1984. The effects of furosemide on the endocochlear potential and auditory-nerve fiber tuning curves in cats. Hear. Res. **14:**305–314.
38. **So, E., T. Kikuchi, K. Ishimaru, Y. Miyabe, and T. Kobayashi.** 2001. Immunolocalization of voltage-gated potassium channel Kv3.1b subunit in the cochlea. Neuroreport **12:**2761–2765.
39. **Treadaway, J., and J. Zuo.** 1998. Mapping of the mouse glutamate receptor δ1 subunit (Grid1) to chromosome 14. Genomics **54:**359–360.
40. **Vetter, D. E., M. C. Liberman, J. Mann, J. Barhanin, J. Boulter, M. C. Brown, J. Saffiote-Kolman, S. F. Heinemann, and A. B. Elgoyhen.** 1999. Role of alpha 9 nicotinic ACh receptor subunits in the development and function of cochlear efferent innervation. Neuron **23:**93–103.
41. **Vetter, D. E., J. R. Mann, P. Wangemann, J. Liu, K. J. McLaughlin, F. Lesage, D. C. Marcus, M. Lazdunski, S. F. Heinemann, and J. Barhanin.** 1996. Inner ear defects induced by null mutation of the isk gene. Neuron **17:**1251–1264.
42. **Wang, Y., K. Hirose, and M. C. Liberman.** 2002. Dynamics of noise-induced cellular injury and repair in the mouse cochlea. J. Assoc. Res. Otolaryngol. **3:**248–268.
43. **Wangemann, P.** 2002. K+ cycling and the endocochlear potential. Hear. Res. **165:**1–9.
44. **Wollmuth, L. P., T. Kuner, C. Jatzke, P. H. Seeburg, N. Heintz, and J. Zuo.** 2000. The Lurcher mutation identifies δ2 as an AMPA/kainate receptor-like channel that is potentiated by Ca^{2+}. J. Neurosci. **20:**5973–5980.
45. **Yamazaki, M., K. Araki, A. Shibata, and M. Mishina.** 1992. Molecular cloning of a cDNA encoding a novel member of the mouse glutamate receptor channel family. Biochem. Biophys. Res. Commun. **183:**886–892.
46. **Yuzaki, M.** 2003. The δ2 glutamate receptor: 10 years later. Neurosci. Res. **46:**11–22.
47. **Zakharenko, S. S., L. Zablow, and S. A. Siegelbaum.** 2001. Visualization of changes in presynaptic function during long-term synaptic plasticity. Nat. Neurosci. **4:**711–717.
48. **Zuo, J., P. L. De Jager, K. A. Takahashi, W. Jiang, D. J. Linden, and N. Heintz.** 1997. Neurodegeneration in Lurcher mice caused by mutation in δ2 glutamate receptor gene. Nature **388:**769–773.